NASA/ONERA Collaboration on Small Hovering Rotor Broadband Noise Prediction using Lattice-Boltzmann Method and Structured Navier-Stokes Solvers

Christopher S. Thurman*, D. Douglas Boyd Jr.†, Pieter G. Buning‡
NASA Langley Research Center, Hampton, VA, 23681

Gabriel Reboul§, Christophe Benoit¶
DAAA, ONERA, Institut Polytechnique de Paris
F-92322 Châtillon, France

This work compares two lattice-Boltzmann method solvers, PowerFLOW and ProLB, and two structured Navier-Stokes solvers, OVERFLOW2 and FAST, used by NASA and ONERA, respectively, for the broadband noise prediction of an ideally twisted rotor as part of Implementing Arrangement number FR-0685-0, 'Comparing Computational Fluid Dynamics Solvers for Broadband Noise Prediction.' Predicted results are evaluated against measured data from both smooth and rough blade sets acquired in the Small Hover Anechoic Chamber at the NASA Langley Research Center. Aerodynamic thrust predictions are seen to agree more favorably with the rough-blade measurements, whereas torque predictions agree better with the smooth-blade measurements. A tonal noise comparison shows better agreement to the measured data with the two structured Navier-Stokes solvers than with the two lattice-Boltzmann solvers, which is thought to be caused by the different geometric discretization associated with each solver paradigm. Broadband noise comparisons show that both lattice-Boltzmann method solvers trend well with the smooth-blade measurements, with the exception of an overprediction by ProLB between 4 kHz and 15 kHz. OVERFLOW2 is seen to capture the measured nondeterministic tonal content between 3 kHz and 8 kHz on a narrowband spectral basis and FAST agrees well with the rough blades on a one-third octave band basis.

Nomenclature

c	=	rotor blade chord length, m
G_{xx}	=	power spectral density, Pa^2/Hz
k	=	turbulent kinetic energy, m^2/s^2
M_{tip}	=	Mach number at the rotor blade tip
N_b	=	number of rotor blades
p_{ref}	=	reference pressure, 20 μPa
R	=	rotor radius, m
Re_{tip}	=	Reynolds number at the rotor blade tip
r	=	rotor blade span location normalized by rotor radius
SPL	=	sound pressure level, dB
$\text{SPL}_{1/3}$	=	one-third octave sound pressure level, dB
y	=	radial observer location relative to the center of rotor rotation normalized by R
Δf	=	narrowband spectra frequency resolution, Hz
ϵ	=	turbulent kinetic energy dissipation rate, m^2/s^3
Θ_{obs}	=	observer angle relative to rotor plane, deg

*Research Aerospace Engineer, Aeroacoustics Branch, AIAA Member; christopher.thurman@nasa.gov
†Senior Research Aerospace Engineer, Aeroacoustics Branch, AIAA Associate Fellow; d.d.boyd@nasa.gov
‡Senior Research Aerospace Engineer, Computational Aerosciences Branch, AIAA Associate Fellow; pieter.g.buning@nasa.gov
§Research Engineer, Aerodynamics, Aeroelasticity and Acoustics Department; gabriel.reboul@onera.fr
¶Research Engineer, Aerodynamics, Aeroelasticity and Acoustics Department, AIAA Member; christophe.benoit@onera.fr

Ω = rotor speed, RPM

I. Introduction

RECENT years have seen considerable interest in advanced air mobility (AAM) vehicles, capable of transporting personnel and packages across various environments in a safe and sustainable way. These vehicles are typically comprised of multirotor systems and generally range in size from small unmanned aerial systems (sUAS) to single- or multipassenger vehicles designed for operation in urban environments. Though the AAM industry is growing at a rapid pace, noise is still a concern for the development and real-world application of these AAM vehicles. Designing AAM vehicles to minimize the acoustic impact on communities has motivated research in identifying and characterizing noise sources produced by sUAS, such as quadcopters. The study of these smaller UAS or their isolated components (i.e., rotors) can aid the design of AAM vehicles with reduced acoustic emissions, mission planning, and trajectory optimization. Due to the limited availability of experimental data, this paper will computationally examine an sUAS rotor to gain a better understanding of larger AAM vehicles.

The large differences in size and operating conditions compared to traditional rotorcraft have led to a paradigm shift in the relative importance of different noise-generating mechanisms. For example, it has been shown that the stochastic, or broadband, portion of the noise emanating from sUAS lies in the most perceptible range of human audibility and may be a dominant noise source when compared to the deterministic, or tonal, noise components [1, 2]. This is in contrast to traditional rotorcraft, where tonal noise dominates over broadband noise. It is for this reason that, to date, limited work has been done toward development for the prediction and analysis of rotor broadband noise.

Many tools exist for predicting both tonal and broadband noise [1, 3–5]. Modeling tonal noise typically entails an aerodynamic calculation to compute blade aerodynamic forces and kinematics and an acoustic propagation code to predict the noise at an observer location. For the aerodynamic calculation, a wide range of tools with varying fidelity exist: panel methods, blade element momentum theory (BEMT), comprehensive analysis codes (e.g., CAMRAD II, CHARM, and RCAS), traditional Navier-Stokes (N-S) solvers (e.g., OVERFLOW2 and FUN3D), and scale-resolving flow simulations (e.g., direct numerical simulations and large eddy simulations (LES)). Each of these tools is used to predict unsteady aerodynamic forces, which are in turn used to predict acoustic pressure at an observer location using an implementation of the Ffowcs Williams and Hawkings (FW-H) equation [6]. Similar approaches have been used to predict broadband noise directly from unsteady aerodynamic forces using the lattice-Boltzmann method (LBM) [3, 4, 7–9], implicit LES [10], and hybrid Reynolds-averaged N-S (RANS)/LES [11–13].

Currently, there is much ambiguity surrounding the prediction of rotor broadband noise using finite-volume N-S solvers. Hybrid RANS/LES paradigms are the workhorse finite-volume method implemented for practical engineering problems; however, the boundary layer is often assumed to be fully turbulent and is modeled using RANS-based turbulence models. This assumption is counterintuitive to the prediction of broadband self-noise sources such as turbulent boundary layer trailing edge noise, because the noise-producing energetic turbulence in the outer region of the boundary layer is being modeled and not resolved. This limitation is not unique to hybrid RANS/LES paradigms and was shown to also be problematic when using wall-functions unless some triggering mechanism (e.g., boundary layer trip) was used to activate the scale-resolving modality in the boundary layer [7, 8, 14]. However, it may be argued that when external turbulence is present, such as blade wake entrained by tip vortices (i.e., blade-wake interaction (BWI) noise), accurate broadband noise predictions can be attained. Furthermore, it was shown in Ref. [11] that hybrid RANS/LES solvers are capable of predicting broadband noise sources such as BWI noise, blade-wake back-scatter noise, bluntness vortex shedding noise, and tip vortex formation noise, which were shown to be dominant noise sources for a small hovering ideally twisted rotor (ITR) geometry at its design operating condition of Ω = 5500 RPM.

The current work serves as a comparison study among different computational fluid dynamics (CFD) solvers used by both NASA and ONERA as part of Implementing Arrangement number FR-0685-0, 'Comparing Computational Fluid Dynamics Solvers for Broadband Noise Prediction' under the NASA-ONERA International Framework Agreement on Cooperation in Civil Aeronautics Research. In this work, two LBM codes, PowerFLOW and ProLB, as well as two structured N-S solvers, OVERFLOW2 and Flexible Aerodynamic Solver Technology (FAST), are used to predict broadband noise from the hovering ITR of Refs. [3] and [15]. Aerodynamic and acoustic predictions are then compared to measured results from the Small Hover Anechoic Chamber (SHAC) facility at the NASA Langley Research Center, and the codes from each participant are evaluated.

II. Technical Approach

A. Rotor Design

The rotor utilized in this work was the four-bladed (N_b = 4) ITR, which is shown in Fig. 1. The ITR has a radius of R = 0.15875 m, uses an NACA 0012 airfoil profile along the blade span, and has a constant chord length of c = 0.0254 m with a blunt trailing edge measuring $0.0157c$. It was designed using BEMT to produce 11.12 N of thrust at a rotor speed of Ω = 5500 RPM (M_{tip} = 0.269, Re_{tip} = 1.98 x 10^5). Further details of the ITR design can be found in Ref. [15].

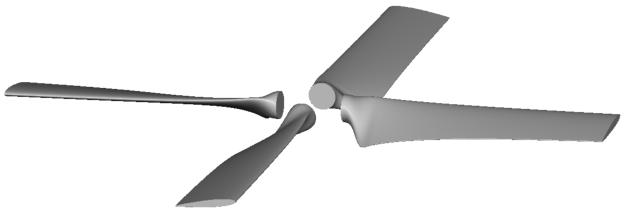

Fig. 1 Ideally twisted rotor geometry.

B. Lattice-Boltzmann Method Solvers

The two LBM solvers compared in this work were PowerFLOW (V6-2020-R3) and ProLB (V2.8.0), with the former being utilized by NASA and the latter by ONERA. Predictions using PowerFLOW on the ITR geometry with both a coarse and fine grid have already been documented in Ref. [3] and the coarse grid results are used for the comparison in this work. Application of ProLB to open rotor configurations is relatively new, specifically at low Reynolds numbers; however, ProLB was recently evaluated by Daroukh et al. [16] using a low-speed turbofan geometry with promising acoustic results. References [17] and [18] provide a detailed theoretical explanation of LBM and only major code details and differences will be discussed herein.

Both PowerFLOW and ProLB utilize LBM in a similar fashion, entailing the use of an 'automatic' grid generator, isotropic Cartesian cells with hanging nodes between different grid resolution regions, an immersed boundary method, wall-functions in the first cell adjacent to the geometry, a rotating grid region encompassing the rotor geometry with trilinear interpolation between stationary and rotating grids, and a form of LES in the off-body volumetric regions. PowerFLOW recalibrates the viscous relaxation time in the Boltzmann equation using a two-equation $k-\epsilon$ renormalization group and ProLB recalibrates the viscous relaxation time using the shear-improved Smagorinsky model of Lévêque et al. [19]. LBM is inherently explicit in time, meaning a local timestep is defined for each cell using the local speed of sound, cell size, and a Courant-Friedrichs-Lewy number of unity. A comparison of the spatiotemporal properties of the simulations conducted using each LBM solver is shown in Table 1, and the computational domain used by ProLB is shown in Fig. 2. It should be noted that the major distinction between the two LBM predictions is that in PowerFLOW, the laminar-to-turbulent transitional wall-function method [20] was used and in ProLB, the fully turbulent wall-function method was used.

Table 1 LBM simulation parameters.

Solver	Number of Voxels	Finest Voxel Size (%c)	Finest Timestep	CPU Hours per Revolution
PowerFLOW	132 million	0.33	0.0053°	2267
ProLB	113 million	0.40	0.0066°	1860

C. Structured Navier-Stokes Solvers

Two structured N-S solvers are also compared in this work, OVERFLOW2 [21] used by NASA and FAST [22, 23] used by ONERA. OVERFLOW2 is a structured-grid N-S solver, which employs an overlapping grid methodology [24]. Full OVERFLOW2 details can be found in Ref. [21]. Exact discretization and numerical details of the OVERFLOW2 ITR simulation can be found in Ref. [11]. This reference showed that using a finer spatial resolution improved broadband noise prediction accuracy on a one-third octave band representation at the cost of narrowband prediction accuracy of mid-frequency nondeterministic tonal content. Because of this, it was thought that the acoustic predictions from Ref. [11], which used the one-equation Spalart-Allmaras (SA) turbulence model with a rotation/curvature correction within the standard delayed detached eddy simulation (DDES) framework [25], predicted the best representation of broadband noise on a narrowband basis and will serve as the OVERFLOW2 case in this work. It should also be noted that adaptive mesh refinement (AMR) was used by OVERFLOW2 in the off-body grids. FAST is also a structured-grid

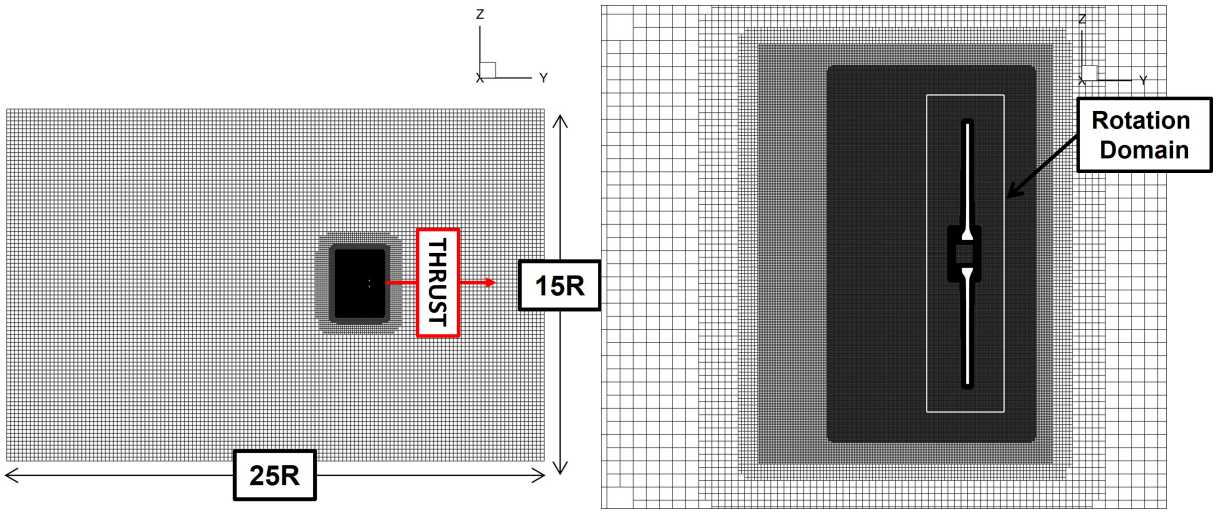

(a) Full computational domain. **(b) Enlarged view of computational domain.**

Fig. 2 ProLB computational domain visualization.

N-S solver, which used an overset technique similar to OVERFLOW2 to rotate the near-body blade grids through the stationary background grid. FAST uses a regular Cartesian core around the rotor with off-body grid spacing gradually increasing away from the Cartesian core. FAST employed the zonal detached eddy simulation (ZDES) of Deck [26], which consisted of using the SA turbulence model with a rotation correction in the boundary layer, and LES elsewhere.

A top view comparison of the blade surface grid can be seen in Fig. 3, where Fig. 3a shows three surface grids used by OVERFLOW2; one encompassing the main portion of the blade and two in red on the tip and root end caps, which overlap the main blade grid. Figure 3b shows the increased spatial resolution of the surface grid used by FAST. In

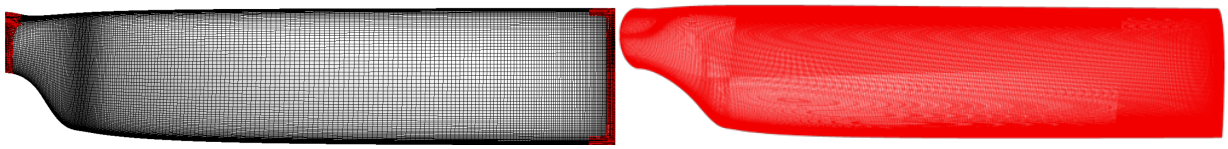

(a) OVERFLOW2. **(b) FAST.**

Fig. 3 Ideally twisted rotor surface grids.

general, it can be said that both OVERFLOW2 and FAST are similar structured N-S solvers, with the main differences being the overlapping grid methodology used by OVERFLOW2, the spatiotemporal resolutions used, and the numerics used for the simulations in this work, which are listed in Table 2. For the spatial discretization used by each solver,

Table 2 Structured Navier-Stokes simulation parameters.

Solver	Number of Grid Points	Mean Surface Cell Size (%c)	Finest Off-Body Cell Size (%c)	Timestep	CPU Hours per Revolution
OVERFLOW2	103 million	2.00	5.00	0.25°	700
FAST	450 million	1.06	1.80	0.125°	6600

OVERFLOW2 used the improved Einfeldt's version of the Harten, Lax, and Van Leer (HLLE++) upwind algorithm [27] with a fifth-order weighted essentially non-oscillatory (WENO5M) flux reconstruction across the entire computational domain, and FAST utilized a third-order monotonic upstream-centered scheme for scalar conservation laws (MUSCL) flux reconstruction with Roe flux difference splitting in the near-body blade grids and the low-dissipation advection

upstream splitting method (AUSM) of Mary and Sagaut [28] in the off-body region. Second-order implicit timestepping was used by both solvers to reduce the pseudo time integration error at each time step.

The spatial resolution differences can be partly explained by the use of AMR by OVERFLOW2, which significantly reduces the cell count when compared to using fixed resolution regions throughout the computational domain. Bearing this in mind, the spatial resolution comparison between OVERFLOW2 and FAST should consider the mean surface and finest off-body cell sizes, which are roughly proportioned two-to-one, with the resolution from FAST being twice as fine as from OVERFLOW2. In general, it can be said that third-order MUSCL flux reconstructions require nearly twice the number of cells to resolve the same content as a WENO5 flux reconstruction [29–31], justifying the disparate spatial resolutions between solvers as being similarly matched, in terms of resolvable content.

D. Acoustic Post-Processing

Unsteady blade loading for each simulation was sampled over approximately eight revolutions once aerodynamic convergence was established. These sampled data were then provided to an FW-H solver for the computation of propagated acoustic pressure time history (APTH) from the impermeable rotor blade surfaces to observer locations. For the ProLB and FAST simulations, the Kirchhoff Integral Method (KIM) code [32] was utilized as an FW-H solver where a forward-time calculation was used. Farassat's Formulation 1A (F1A) [33–35] was used to solve the FW-H equation for both PowerFLOW using PowerACOUSTICS and OVERFLOW2 using the ANOPP2 [36] CFD Acoustic Propagation Tool (ACAPT).

The calculated APTH from the eight revolutions of sampled data was separated into eight equally sized blocks corresponding to each revolution of rotor data. These eight revolutions of data were averaged together to obtain a mean revolution of APTH, which is the periodic (i.e., tonal) acoustic component. This periodic acoustic component was then subtracted from the raw, aperiodic APTH from the eight revolutions of data and the resultant residual APTH served as the stochastic (i.e., broadband) acoustic component. The following acoustic processing methods were then used and are similar to those used for the experimental data measured in the SHAC facility at the NASA Langley Research Center [15]:

1. The mean rotor revolution of predicted data was repeated enough times to attain a $\Delta f = 20$ Hz frequency resolution, which was then processed by treating the repeated rotor revolution data as an aperiodic signal, computing the fast Fourier transform (FFT) of the data with a Hanning window and no overlap, then using Eq. (1) to produce a narrowband spectrum of the predicted tonal noise sound pressure level (SPL);

$$\mathrm{SPL} = 10\log_{10}\left(\frac{G_{xx} * \Delta f}{p_{\mathrm{ref}}^2}\right), \tag{1}$$

   where G_{xx} is the resultant power spectral density from the FFT calculation and $p_{\mathrm{ref}} = 20\ \mu$Pa.

2. For establishing tonal directivity patterns, the mean revolution of APTH was filtered using a second-order Butterworth narrow bandpass filter with a ±20 Hz frequency band centered on the fundamental blade passage frequency (BPF). This filter served the purpose of mitigating spectral leakage associated with different measurement and post-processing techniques. The root mean squared value of these filtered data, $\bar{p}_{rms}$, was used to calculate the amplitude of the fundamental BPF on a logarithmic basis using:

$$\mathrm{SPL}_{\mathrm{BPF}} = 20\log_{10}\left(\frac{\bar{p}_{\mathrm{rms}}}{p_{\mathrm{ref}}}\right). \tag{2}$$

3. The extracted broadband noise signals from the computations were treated as aperiodic signals over which an FFT using a Hanning window with 50% overlap was also calculated using eight blocks, or one block per revolution of residual APTH data, resulting in a spectral resolution of $\Delta f = 91.68$ Hz. Equation (1) was used to produce narrowband stochastic noise SPL values, which were then used to generate autospectral and one-third octave band ($\mathrm{SPL}_{1/3}$) representations.

III. Aerodynamic Performance Results

The computed thrust and torque values using the LBM and structured N-S solvers are compared against measured data in Table 3. For the experimental data, measurements from both the smooth stereolithography (SLA) and rough selective

laser sintering (SLS) blade sets of Ref. [15] are shown. The SLA blades were thought to have a laminar-to-turbulent transitional boundary layer and the SLS blades, a fully turbulent boundary layer. Though the wall-treatment for all but the PowerFLOW simulation used a fully turbulent assumption, it is thought that the lack of predicted boundary layer eddies in a wall-model or RANS framework would produce a boundary layer character more closely aligned with the SLA blades; however, force and moment predictions using a fully turbulent assumption may be better suited for comparison against the SLS blades. In general, it can be said that all thrust predictions compare better with the SLS blades and all torque predictions compare better with the SLA blades.

Table 3 Aerodynamic performance comparison at the design operating condition.

Case	Experiment		Lattice-Boltzmann Solvers		Structured Navier-Stokes Solvers	
	SLA	SLS	PowerFLOW	ProLB	OVERFLOW2	FAST
Thrust	10.1 N	9.51 N	9.08 N	8.96 N	9.30 N	9.55 N
Relative Diff.			10.1%/4.52%	11.3%/5.78%	7.92%/2.21%	5.45%/-0.421%
Torque	-0.213 N-m	-0.242 N-m	-0.173 N-m	-0.210 N-m	-0.209 N-m	-0.209 N-m
Relative Diff.			18.8%/28.5%	1.41%/13.2%	1.88%/13.6%	1.88%/13.6%

It can be seen in the table that the two LBM codes predict very similar thrust values when compared to the experiment. ProLB does a much better job at predicting torque; however, as mentioned previously, ProLB used fully turbulent wall-functions, whereas laminar-to-turbulent transitional wall-functions were used by PowerFLOW. One would expect an increased skin friction prediction from using fully turbulent wall-functions, which may explain the more accurate torque prediction by ProLB. Both OVERFLOW2 and FAST also model the boundary layer as fully turbulent with RANS, explaining their similar torque prediction when compared to the ProLB results. Similar predictions for thrust and torque can be seen from both structured N-S solvers when compared to the measured data, with a slightly more accurate thrust prediction from FAST. Both structured N-S solvers predict thrust more accurately than the LBM solvers when compared to the measured data, possibly due to a better geometric resolution when using body-fitted grids rather than an immersed boundary method approach.

IV. Aeroacoustic Results

Total noise spectra from Pettingill et al. [15] for the smooth SLA and rough SLS blades at an out-of-plane observer located $\Theta_{obs} = -35°$ below the rotor plane and $y = 11.94R$ away from the rotor are shown in Fig. 4. It can be seen

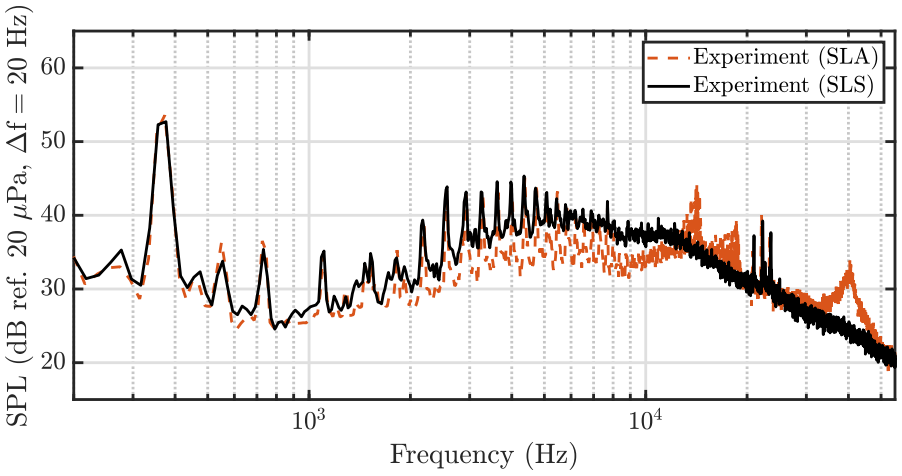

Fig. 4 Comparison of measured data at the out-of-plane observer location ($\Theta_{obs} = -35°$, $y = 11.94R$).

that there are minor differences at the BPF and its harmonics between measured data. Broadband noise between approximately 2 kHz and 8 kHz appears to have similar nondeterministic residual tonal peaks; however, the trough

amplitudes of these residual tones are elevated for the rough SLS blades when compared to the SLA blades, likely due to the blade boundary layer differences discussed previously.

A. Tonal Noise

The first acoustic processing method was used to produce a tonal noise comparison between the predictions and measured data on an SPL narrowband basis in Fig. 5 at an out-of-plane observer located $\Theta_{obs} = -35°$ below the rotor plane and $y = 11.94R$ away from the rotor. Because the tonal noise was nearly identical between the SLA and SLS blades as shown in Fig. 4, only the measured tonal noise data from the SLA blades are shown in this section. It was

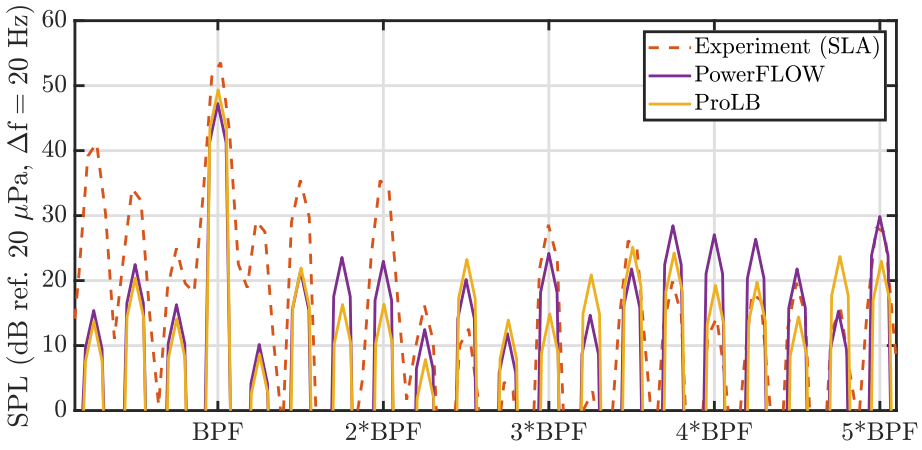

(a) Lattice-Boltzmann comparison.

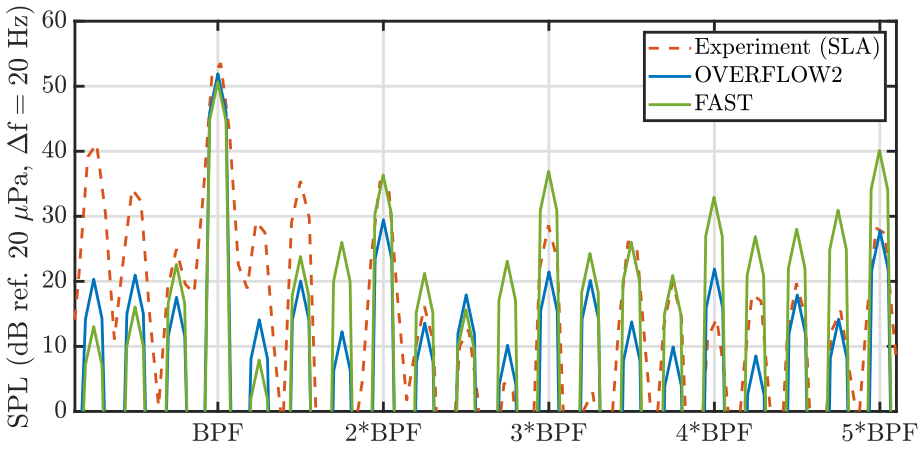

(b) Structured Navier-Stokes comparison.

Fig. 5 Tonal noise narrowband spectra at the out-of-plane observer location ($\Theta_{obs} = -35°$, $y = 11.94R$).

shown in Ref. [15] that the ITR tonal noise at the fundamental BPF is thickness noise dominant, implying that accurate prediction of the BPF relies heavily on geometric discretization and kinematics of the rotor blades. Because both LBM solvers use an immersed boundary method and isotropic Cartesian cells, the volumetric spatial resolution dictates how well the geometry is resolved by the 'automatic' grid generator in the solver. Both LBM simulations had very similar spatial resolutions, explaining their similar prediction accuracy of the BPF when compared to the measured data. This postulation is further supported by Ref. [11], where a PowerFLOW simulation of the ITR using a finer spatial resolution predicted a more accurate BPF amplitude compared to the smooth SLA blades. Because the structured N-S computational domains contain stretched body-fitted grids that approach very near to the rotor blade surfaces, which are also discretized with surface grids, there is more control of how well the geometry is resolved when compared to the

LBM solvers used in this work. Both structured N-S solvers can be seen to predict nearly identical fundamental BPF amplitudes in Fig. 5b and with much better agreement to the measured data than the LBM predictions shown in Fig. 5a. This figure also shows that FAST predicts the first BPF harmonic (i.e., 2*BPF) more accurately than OVERFLOW2.

The second acoustic processing method was used to establish directivity trends of the predicted fundamental BPF, which are compared against experimental data in Fig. 6 to gain insight on prediction accuracy across multiple observer locations. It can be seen in Fig. 6a that both LBM solvers underpredict the measured BPF, with ProLB comparing more accurately with the experiment than PowerFLOW. Both structured N-S solvers predict almost identical BPF directivity

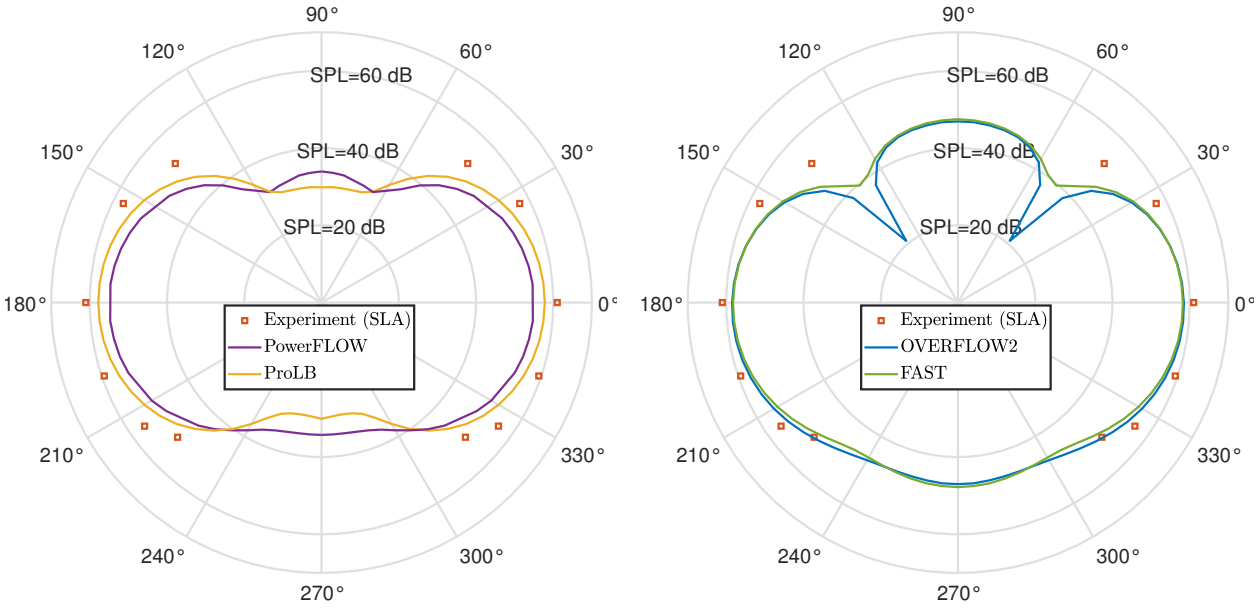

(a) Lattice-Boltzmann comparison. **(b) Structured Navier-Stokes comparison.**

Fig. 6 Fundamental BPF directivity at $y = 11.94R$ ($\Theta_{obs} = 90°$ is directly above the rotor).

patterns in Fig. 6b, including the acoustic null region around $\Theta_{obs} = 50°$, which was not predicted by the LBM codes in Fig. 6a. In general, it can be said that the structured N-S solvers outperform the LBM codes in terms of BPF prediction. All predicted results shown here trend well with the measured data.

B. Broadband Noise

Broadband noise spectra on both a narrowband and $SPL_{1/3}$ basis were produced using the third acoustic processing method and are shown in Fig. 7 for measured data and results predicted using the two LBM solvers at the out-of-plane observer. Because Fig. 4 shows similar nondeterministic tonal content between the smooth SLA and rough SLS blades, only the smooth SLA blades are shown for the narrowband comparisons in this section to keep the figures orderly. Figure 7 shows an overprediction from ProLB between approximately 4 kHz and 15 kHz, with excellent agreement to the smooth SLA blades outside of this frequency range. The PowerFLOW prediction can be seen to agree well with the smooth SLA blades at most frequencies prior to the spectral roll-off around 11 kHz. It should be noted that better agreement was shown between the smooth SLA blades and a PowerFLOW simulation with a finer spatial resolution in Ref. [3]. It can be seen in Fig. 7b that both LBM predictions trend better with the smooth SLA blades than with the rough SLS blades except above 11 kHz for PowerFLOW and between 4 kHz and 15 kHz for ProLB, which may be explained by the absence of predicted boundary layer eddies due to using wall-functions in the first cell adjacent to the geometry. The narrowband representation of the broadband noise in Fig. 7a shows that many of the residual tones between 2 kHz and 8 kHz are not adequately captured by either LBM solver; however, ProLB does a better job at predicting the peak of these features between 3 kHz and 5 kHz.

A similar comparison between the structured N-S solvers and measured data is shown in Fig. 8 at the out-of-plane observer. Figure 8a shows that OVERFLOW2 captures both the peaks and troughs of the residual tones observed in the measured data between 3 kHz and 8 kHz and also predicts the two tone-like structures above 10 kHz, though at different frequencies than in the measured data. It can also be seen that some of the residual tones are not well captured by FAST;

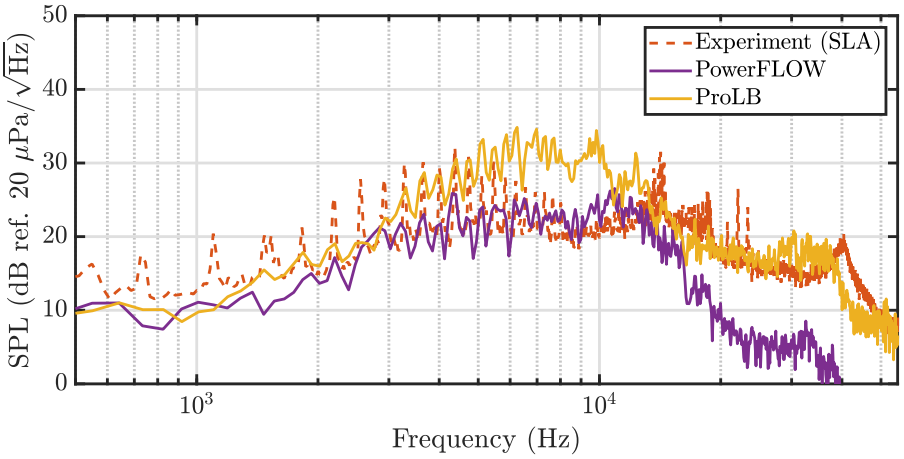

(a) Broadband noise narrowband autospectra.

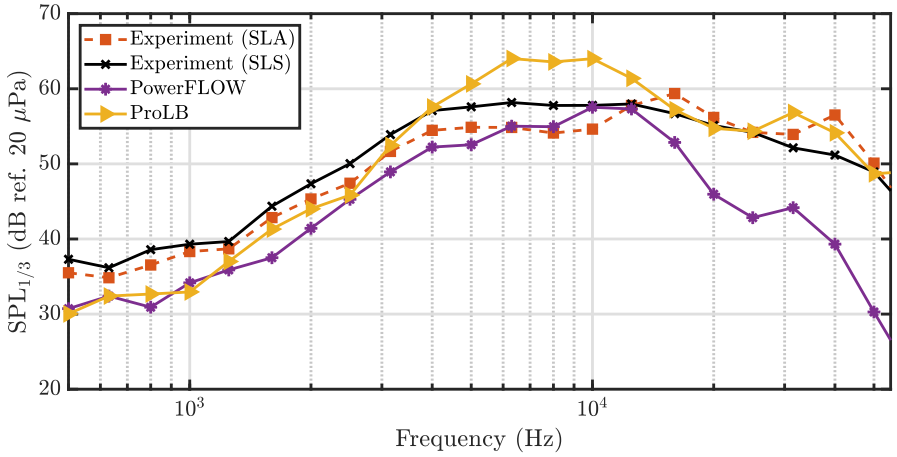

(b) Broadband noise one-third octave spectra.

Fig. 7 Lattice-Boltzmann solver broadband noise comparison at the out-of-plane observer location ($\Theta_{obs} = -35°$, $y = 11.94R$).

however, Fig. 8b shows that, in general, the FAST broadband noise prediction trends well with the rough SLS blade measurement. It should be mentioned that the OVERFLOW2 simulation case chosen from Ref. [11] was selected based upon its ability to capture the residual tones on a narrowband spectral basis and that the finer spatial resolution case, not shown in this work, more accurately captures the broadband noise on a one-third octave band spectral basis.

V. Conclusions

This work compared two lattice-Boltzmann method solvers and two structured Navier-Stokes solvers used by NASA and ONERA for the prediction of aerodynamic performance, tonal noise, and broadband noise of an ideally twisted rotor at its baseline hover operating condition of $\Omega = 5500$ RPM. Results were compared against measured data from both smooth SLA blades and rough SLS blades, which were thought to have different boundary layer characteristics (i.e., transitional vs. fully turbulent). Aerodynamic thrust predictions were seen to compare well with the rough SLS blades, whereas the torque predictions compared better with the smooth SLA blades. Both structured Navier-Stokes solvers, OVERFLOW2 and FAST, showed similar aerodynamic performance predictions. In contrast, the two lattice-Boltzmann method solvers, PowerFLOW and ProLB, predicted larger thrust and torque errors compared to the measured data. The torque prediction from ProLB agreed much better with the structured Navier-Stokes solvers than the PowerFLOW prediction, likely due to the use of fully turbulent wall-functions by ProLB compared to the laminar-to-turbulent

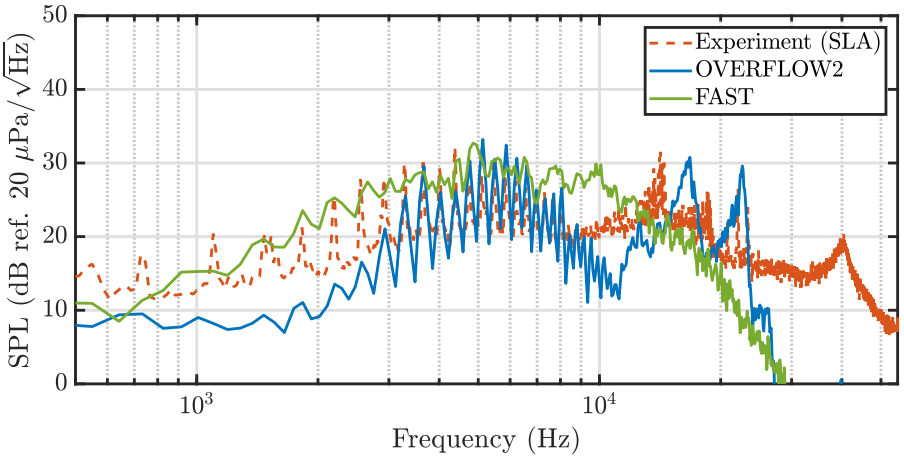

(a) Broadband noise narrowband autospectra.

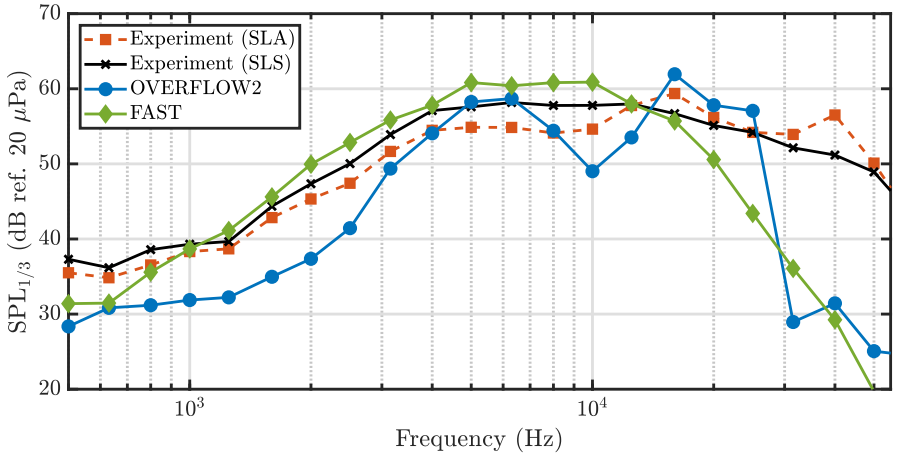

(b) Broadband noise one-third octave spectra.

Fig. 8 Structured Navier-Stokes solver broadband noise comparison at the out-of-plane observer location ($\Theta_{obs} = -35°$, $y = 11.94R$).

transitional wall-functions implemented in PowerFLOW.

A tonal noise comparison between the predictions and smooth SLA blade measurements at an out-of-plane observer location showed that both lattice-Boltzmann method codes underpredicted the fundamental blade passage frequency compared to the structured Navier-Stokes solvers. This underprediction was thought to be due to inadequate geometric discretization caused by using an immersed boundary method with isotropic Cartesian grid cells rather than stretched body-fitted grids, like those used by both structured Navier-Stokes solvers. It was also shown that FAST predicted the first harmonic of the blade passage frequency more accurately than OVERFLOW2 when compared to the measured data. Directivity plots of the fundamental blade passage frequency showed nearly identical directivities from both structured Navier-Stokes solvers, including the prediction of an acoustic null region around $\Theta_{obs} = 50°$. This acoustic null region was not predicted by either lattice-Boltzmann method code; however, all codes trended reasonably well to the measured data with PowerFLOW underpredicting the tonal noise directivity compared to the other three solvers.

Lastly, a broadband noise comparison showed that the two lattice-Boltzmann method solvers trended well with the smooth SLA blades; however, ProLB results were overpredicted between approximately 4 kHz and 15 kHz, whereas a spectral roll-off around 11 kHz was observed for PowerFLOW. It was shown that neither lattice-Boltzmann method solver captured the nondeterministic tonal content between 2 kHz and 8 kHz, but ProLB did predict the peak amplitudes of some residual tones between 3 kHz and 5 kHz. OVERFLOW2 was the only solver capable of predicting this

mid-frequency nondeterministic tonal content on a narrowband basis; however, it showed poor agreement with measured data on a one-third octave band basis. Although the mid-frequency tonal content was not captured by FAST, the broadband noise predicted by this structured Navier-Stokes solver was shown to agree well with the rough SLS blades on a one-third octave band basis.

VI. Acknowledgments

The authors would like to thank Nikolas Zawodny and Nicole Pettingill from the Aeroacoustics Branch at the NASA Langley Research Center for their invaluable role in providing experimental measurements used for comparison in this work. NASA contributions were funded by the NASA Revolutionary Vertical Lift Technology (RVLT) project. NASA computational resources supporting this work were provided by the Midrange HPC K-Cluster at the NASA Langley Research Center.

References

[1] Zawodny, N. S., Boyd Jr., D. D., and Burley, C. L., "Acoustic Characterization and Prediction of Representative, Small-Scale Rotary-Wing Unmanned Aircraft System Components," *AHS International 72nd Annual Forum & Technology Display*, West Palm Beach, FL, May 2016.

[2] Greenwood, E., Brentner, K. S., Rau, R. F., and Ted Gan, Z. F., "Challenges and Opportunities for Low Noise Electric Aircraft," *International Journal of Aeroacoustics*, Vol. 21, No. 5–7, 2022, pp. 315–381.

[3] Thurman, C. S., Zawodny, N. S., Pettingill, N. A., Lopes, L. V., and Baeder, J. D., "Physics-informed Broadband Noise Source Identification and Prediction of an Ideally Twisted Rotor," *AIAA SciTech 2021 Forum*, AIAA Paper 2021–1925, Virtual, January 2021.

[4] Thurman, C. S., Zawodny, N. S., and Baeder, J. D., "Computational Prediction of Broadband Noise from a Representative Small Unmanned Aerial System Rotor," *VFS International 76th Annual Forum & Technology Display*, Virtual, October 2020.

[5] Li, S., and Lee, S., "UCD-QuietFly: A New Program to Predict Multi-Rotor eVTOL Broadband Noise," *2020 VFS Aeromechanics for Advanced Vertical Flight Technical Meeting*, San Jose, CA, January 2020.

[6] Ffowcs Williams, J. E., and Hawkings, D. L., "Sound Generation by Turbulence and Surfaces in Arbitrary Motion," *Philosophical Transactions of the Royal Society of London. Series A, Mathematical and Physical Sciences*, Vol. 264, No. 1151, 1969, pp. 321–342.

[7] Thurman, C. S., "Computational Study of Boundary Layer Effects on Stochastic Rotor Blade Vortex Shedding Noise," *Aerospace Science and Technology*, Vol. 131A, No. 107983, 2022.

[8] Casalino, D., Romani, G., Zhang, R., and Chen, H., "Lattice-Boltzmann Calculations of Rotor Aeroacoustics in Transitional Boundary Layer Regime," *Aerospace Science and Technology*, Vol. 130, No. 107953, 2022.

[9] Casalino, D., Romani, G., Maria Pii, L., and Colombo, R., "Sensitivity of Laminar Separation Noise from a Rotor to Inflow Turbulence," *AIAA AVIATION 2023 Forum*, AIAA Paper 2023–3220, San Diego, CA, June 2023.

[10] Kunz, F. T., Pullin, S., Zhou, B. Y., Azarpeyvand, M., Galimberti, L., Morelli, M., and Guardone, A., "High-Fidelity Propeller Broadband Noise Prediction using SU2," *AIAA AVIATION 2023 Forum*, AIAA Paper 2023–4185, San Diego, CA, June 2023.

[11] Thurman, C. S., Boyd Jr., D. D., and Lopes, L. V., "Prediction of Broadband Blade-Wake Back-Scatter Noise from a Hovering Ideally Twisted Rotor using OVERFLOW2-ANOPP2," *AIAA SciTech 2024 Forum*, AIAA Paper 2024–2471, Orlando, FL, January 2024.

[12] Mankbadi, R. R., Afari, S. O., and Golubev, V. V., "High-Fidelity Simulations of Noise Generation in a Propeller-Driven Unmanned Aerial Vehicle," *AIAA Journal*, Vol. 59, No. 3, 2021, pp. 1020–1039.

[13] Broatch, A., Navarro, R., García-Tíscar, J., and Ramírez, F. N., "Evaluation of Different FW-H Surfaces and Modal Decomposition Techniques for the Acoustic Analysis of UAV Propellers through Detached Eddy Simulations," *Aerospace Science and Technology*, Vol. 146, No. 108956, 2024.

[14] Thurman, C. S., Zawodny, N. S., and Pettingill, N. A., "The Effect of Boundary Layer Character on Stochastic Rotor Blade Vortex Shedding Noise," *VFS International 78th Annual Forum & Technology Display*, Fort Worth, TX, May 2022.

[15] Pettingill, N. A., Zawodny, N. S., Thurman, C. S., and Lopes, L. V., "Acoustic and Performance Characteristics of an Ideally Twisted Rotor in Hover," *AIAA SciTech 2021 Forum*, AIAA Paper 2021–1928, Virtual, January 2021.

[16] Daroukh, M., Le Garrec, T., and Polacsek, C., "Low-Speed Turbofan Aerodynamic and Acoustic Prediction with an Isothermal Lattice Boltzmann Method," *AIAA Journal*, Vol. 60, No. 2, 2022, pp. 1152–1170.

[17] Succi, S., *The Lattice Boltzmann Equation for Fluid Dynamics and Beyond*, 1st ed., Clarendon Press, Oxford, 2001.

[18] Shan, X., Yuan, X.-F., , and Chen, H., "Kinetic Theory Representation of Hydrodynamics: a Way Beyond the Navier-Stokes Equation," *Journal of Fluid Mechanics*, Vol. 550, 2006, pp. 413–441.

[19] Lévêque, E., Toschi, F., Shao, L., and Bertoglio, J.-P., "Shear-Improved Smagorinsky Model for Large-Eddy Simulation of Wall-Bounded Turbulent Flows," *Journal of Fluid Mechanics*, Vol. 570, 2007, pp. 491–502.

[20] Duda, B., Fares, E., Kotapati, R., Li, Y., Staroselsky, I., Zhang, R., and Chen, H., "Capturing Laminar to Turbulent Transition within the LBM based CFD solver PowerFLOW," *AIAA SciTech 2019 Forum*, AIAA Paper 2019–1832, San Diego, CA, January 2019.

[21] Nichols, R. H., Tramel, R. W., and Buning, P. G., "Solver and Turbulence Model Upgrades to OVERFLOW 2 for Unsteady and High-Speed Applications," *24th Applied Aerodynamics Conference*, AIAA Paper 2006–2824, San Francisco, CA, June 2006.

[22] Dandois, J., Mary, I., and Brion, V., "Large-eddy Simulation of Laminar Transonic Buffet," *Journal of Fluid Mechanics*, Vol. 850, 2018, pp. 156–178.

[23] Suss, A., Mary, I., Le Garrec, T., and Marié, S., "Comprehensive Comparison between the Lattice Boltzmann and Navier-Stokes Methods for Aerodynamic and Aeroacoustic Applications," *Computers and Fluids*, Vol. 257, No. 105881, 2023.

[24] Benek, J. A., Buning, P. G., and Steger, J. L., "A 3-D CHIMERA Grid Embedding Technique," *7th Computational Physics Conference*, AIAA Paper 85–1523, Cincinnati, OH, July 1985.

[25] Spalart, P. R., Deck, S., Shur, M. L., Squires, K. D., Strelets, M. K., and Travin, A., "A New Version of Detached-eddy Simulation, Resistant to Ambiguous Grid Densities," *Theoretical and Computational Fluid Dynamics*, Vol. 20, 2006, pp. 181–195.

[26] Deck, S., "Zonal-Detached-Eddy Simulation of the Flow Around a High-Lift Configuration," *AIAA Journal*, Vol. 43, No. 11, 2005, pp. 2372–2384.

[27] Tramel, R. W., Nichols, R. H., and Buning, P. G., "Addition of Improved Shock-Capturing Schemes to OVERFLOW 2.1," *19th AIAA Computational Fluid Dynamics Conference*, AIAA Paper 2009–3988, San Antonio, TX, June 2009.

[28] Mary, I., and Sagaut, P., "Large Eddy Simulation of Flow around an Airfoil Near Stall," *AIAA Journal*, Vol. 40, No. 6, 2002, pp. 1139–1145.

[29] Chamarthi, A. S., Hoffmann, N., Nishikawa, H., and Frankel, S. H., "Implicit Gradients Based Conservative Numerical Scheme for Compressible Flows," *Journal of Scientific Computing*, Vol. 95, No. 17, 2023.

[30] Ghosh, D., Medida, S., and Baeder, J. D., "Compact-Reconstruction Weighted Essentially Non-Oscillatory Schemes for the Unsteady Navier-Stokes Equations," *42nd AIAA Fluid Dynamics Conference and Exhibit*, AIAA Paper 2012–2832, New Orleans, LA, June 2012.

[31] Sun, Y., Shi, Y., and Xu, G., "Application of High-Order WENO Scheme in the CFD/FW–H Method to Predict Helicopter Rotor Blade–Vortex Interaction Tonal Noise," *Aerospace*, Vol. 9, No. 4, 2022.

[32] Prieur, J., and Rahier, G., "Aeroacoustic Integral Methods, Formulation and Efficient Numerical Implementation," *Aerospace Science and Technology*, Vol. 5, No. 7, 2001, pp. 457–468.

[33] Farassat, F., and Succi, G. P., "The Prediction of Helicopter Discrete Frequency Noise," *Vertica*, Vol. 7, No. 4, 1983, pp. 309–320.

[34] Brentner, K., and Farassat, F., "Modeling Aerodynamically Generated Sound of Helicopter Rotors," *Progress in Aerospace Sciences*, Vol. 39, No. 2–3, 2003, pp. 83–120.

[35] Lopes, L., "ANOPP2's Farassat Formulations Internal Functional Modules (AFFIFMs) Reference Manual," NASA TM 20210021111, 2021.

[36] Lopes, L., and Burley, C., "ANOPP2 User's Manual: Version 1.2," NASA TM 2016-219342, 2016.